Exact diagonalization and Quantum Monte Carlo studies of quantum dots

A.D. Güçlü and Hong Guo[a]

[a]Center for the Physics of Materials and Department of Physics, McGill University, Montreal, PQ, Canada H3A 2T8

We report exact diagonalization and diffusion quantum Monte Carlo calculations of quantum dots (QDs) in which energetics due to electron-electron interactions, magnetic field, and geometrical factors compete and induce interesting ground state configurations. The geometrical effects are generated by different confining potentials such as parabolic shaped, ring shaped, and disordered potentials. The addition spectra, spin configurations and Hund's rules are investigated for QDs containing up to 13 strongly interacting electrons. In addition to the familiar Coulomb and spin blockades, a new transport blockade is predicted when the electrons are spatially localized in different potential minima. While the transition energy between spin states is found to be affected by the disorder, closed shell Hund's rule is maintained for the disorder strength considered here.

Nous avons effectué des calculs de diagonalisation exacte et de Monte-Carlo quantique sur des points quantiques (QD) dans lesquels le bilan énergétique impliquant les interactions électron-électron, le champ magnétique et des facteurs géométriques sont en compétition et produisent des états fondamentaux intéressants. Les effets géométriques sont déterminés par la forme du potentiel de confinement (parabolique ou en anneau) et du potentiel de désordre. Les spectres d'addition, les configurations de spin et les règles de Hund sont étudiés pour des points quantiques comportant jusqu'à 13 électrons en forte interaction. En plus du blocage de Coulomb et de spin, un nouveau blocage de transport est prédit lorsque les électrons sont localisés dans l'espace sur des minimums différents du potentiel. Alors que l'énergie de transition entre les états de spin est affectée par le désordre, la règle de Hund sur les couches fermées est encore valable pour les degrés de désordre considérés ici.

1 Introduction

Quantum dots (QD) has attracted much attention experimentally and theoretically as they provide a high level of control for electron dynamics and correlation[1–5]. QD's are also called artificial atoms because they have many properties similar to an atom. For instance it is now possible to experimentally determine the atomic-like properties of QD's such as the addition energy, shell structure and spin configurations. Due to the experimental accessibility, QD systems will continue to provide a crucial testing ground for many important concepts of mesoscopic and nanoscopic physics. On the theoretical side, the most accurate treatment of QD's is based on exact diagonalization of the QD Hamiltonian[6–12]. Since computational cost grows exponentially with the electron number N, exact diagonalization is so far limited to highly symmetric QD systems with small number of electrons ($N < 7$). Indeed, conservation of total angular momentum and total spin makes possible to reduce the many-body Hamiltonian of a circular QD system into smaller matrices which can be calculated by parallel computation techniques. Typical size of matrices needed to reach the convergence of a 5 electrons system is about 30000×30000. Larger systems require approximations such as tight-binding[13,14] models. For a qualitative understanding of some properties of QD's, mean-field approximations such as Hartree-Fock[15–24] and density functional theory[25–31] may be used. It is however recognized that in strongly correlated systems, these mean-field approximations can give substantial errors in energy and many-body wave function. A more accurate alternative is quantum Monte Carlo (QMC) methods[32–48] which treat correlation effects exactly while keeping the amount of computation to rise as $\sim O(N^3)$. QMC can be used to study QD systems which do not have a particular spatial symmetry. Indeed, problems lacking spatial symmetry make exact diagonalization calculation powerless if not impossible. Unlike the exact diagonalization technique, QMC method does not require a lot of memory since there is no need of matrix conversion. Computation time is the most important factor in QMC simulations, and this method is well suited for parallel computation techniques.

Experimental investigations[49–53] have provided clear indications that the confining potential landscape can play an essential role to the many-body states of the QD. Several theoretical analysis have been reported in order to elucidate geometrical effects coming from random disorder[13,14, 17,20,21,30,31], chaotic dots[18,23], QD molecules[12,19, 32], non-circular dots[28,29], impurities[34,35], and ring shaped dots[58–61]. Despite the many contributions so far, electron correlation and ground state properties of disordered QD systems remain an active subject of study.

It is the purpose of this paper to report our investigation of geometrical factors in QD's under an external uniform magnetic field. Using an exact diagonalization technique in a continuous potential landscape, with up to five confined electrons. An exact calculation on the energetics of interaction, magnetic field, and geometry is very valuable for elucidating many-body phenomena in QDs. In particular, this model allows us to observe and understand electron charging properties and transport characteristics of QDs under the influence of wave function localization and charge blockade effects.

In order to study the effects of symmetry breaking random disorder we use a diffusion QMC (DQMC) numerical procedure. To the best of our knowledge, QMC analysis of QD's containing impurities have been limited to 2 electrons[34,35], and we are not aware of any previous exact

calculations on energetics and spin configurations of completely disordered QD's up to $N = 13$. Moreover, our DQMC data allows us to probe the physics of clean QD's under external magnetic field with larger number of electrons than studied before. We focus on investigating the competing energetics of electron-electron interaction, magnetic field, and disorder.

2 Model and Method

We consider cylindrically symmetric QDs with a parabolic confinement potential to which we add a distortion potential, and an uniform magnetic field B in the z direction. In the effective mass approximation, single particle Hamiltonian of this system is

$$\begin{aligned} H_0 &= \frac{1}{2m^*}\left(\mathbf{p} - \frac{e}{c}\mathbf{A}(\mathbf{r})\right)^2 + \frac{1}{2}m^*\omega_0^2\mathbf{r}^2 \\ &+ g^*\mu_B B s + V_d(\mathbf{r}), \end{aligned} \quad (1)$$

where m^* is the effective mass of electron, $\mathbf{A}$ is the vector potential, ω_0 is the parameter characterizing the parabolic part of the confinement potential of the QD, g^* is the effective Landé factor. The parabolic confining potential is distorted by a function $V_p(\mathbf{r})$. The solutions to the parabolic part of the confinement potential are the well known Fock-Darwin states, which will be used as basis set through this work.

2.1 Exact Diagonalization

When the function $V_d(\mathbf{r})$ is a radial barrier potential creating two distinct potential regions (a ring region and a core region), the system remains cylindrically symmetric. The total angular momentum is then conserved and an exact diagonalization technique is suitable to study electronic properties of such system. To calculate the many-body states of the interacting electrons, we start from the second-quantized form of the isolated QD Hamiltonian,

$$H_{QD} = \sum_i \epsilon_i c_i^\dagger c_i + \frac{1}{2}\sum_{ijkl} V_{ijkl} c_i^\dagger c_j^\dagger c_l c_k, \quad (2)$$

where ϵ_i is the *single* electron energy level corresponding to the single-particle state labeled by quantum indices (n_i, m_i, σ_i). c ($c^\dagger$) is the annihilation (creation) operator and V_{ijkl} are the Coulomb interaction matrix elements given by

$$\begin{aligned} V_{ijkl} &= \frac{e^2}{\epsilon}\int dx_1 dx_2 \\ &\times \psi_i^*(x_1)\psi_j^*(x_2)\frac{1}{|\mathbf{r}_1 - \mathbf{r}_2|}\psi_k(x_1)\psi_l(x_2), \end{aligned} \quad (3)$$

where the integration includes the summation over spin states. Here, ψ_i are the eigenstates of the single-electron Hamiltonian (which includes $V_d(r)$). We note that, if one is interested in a distortion-free QD with the z-direction neglected, V_{ijkl} do not depend on B apart from a rescaling factor. In our case, however, numerical calculations of the V_{ijkl} must be performed for every value of magnetic field, which is a computationally intensive process. We calculated twenty one points between $B = 0$ and 9 tesla. Exact diagonalization of the many-body Hamiltonian is performed up to $N = 5$ electrons. In addition to the total spin in z-direction S_z, total angular momentum M is a good quantum number due to the cylindrical symmetry of the QD. Therefore, the many-body Hamiltonian can be separated into subspaces with different (M,S_z) configurations. The ground state and lowest excited states are calculated by diagonalizing each subspace using the standard Lanczos procedure for larger matrices.

2.2 Diffusion quantum Monte Carlo

In order to study completely disordered systems, we now consider the distortion function $V_d(\mathbf{r})$ to be a sum of Gaussian profiles with randomly chosen position, width and strength. Since the total angular momentum M is no longer conserved for this system, exact diagonalization becomes powerless. Thus, we consider the many-body Hamiltonian in real space, $H_{QD} = \sum H_0 + H_I$ where H_I is the Coulomb interaction between electrons, and we apply a diffusion quantum Monte Carlo technique. The accuracy of DQMC depends largely on the quality of trial wave functions. Several different trial functions have been used in the literature, including solutions by local density approximation[40], single- or multiple-configuration states of non-interacting electrons[33], optimized with Jastrow factors. Our DQMC method uses unrestricted Hartree-Fock (UHF) solutions as trial states. Since spatial symmetry is broken by disorder, it is unclear *a priori* how to make assumptions on the form of trial wave function. We expect UHF solutions to be a good starting point as we have checked (see below) by comparing DQMC solutions using UHF trial states with exact diagonalization in a disorder-free QD: a very good agreement is found.

The presence of impurities in the Hamiltonian H adds a new degree of complexity to DQMC, because UHF solutions become complex numbers even at zero magnetic field. Since QMC methods can only deal with positive real numbers, a fixed-phase approximation[46,33], which is a generalization of the fixed-node approximation[48], must be used. In the fixed phase approximation, the exact solution of the many-body problem is assumed to have the same phase as the trial wave function. This approximation was introduced[46] to deal with the 2D electron gas and later applied to clean QD's[33], in the presence of a magnetic field. The application of the fixed-phase approximation to disordered QD is technically similar and we refer interested readers to these two references[46,33].

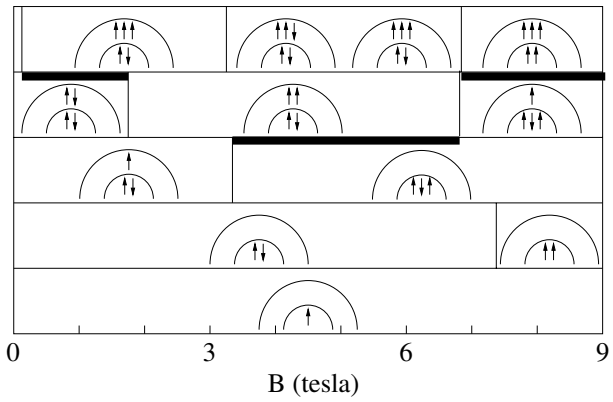

Figure 1. Many-body ground states up to 5 electrons as a function of B, for a strongly distorted QD. The QD is schematized by an inner disc representing the core region and an outer ring representing the peripheral potential minimum. Thick lines represent blockaded regions during a transport measurement. The arrows indicate spin configuration of the electrons. For simplicity, only those states with equivalent localization-spin configuration representing more than 95% contributions to the exact ground state for $B < 3$ tesla, and more than 99.9% contributions for $B > 3$ tesla, are shown. For this QD, the transition from $N = 3$ to $N = 4$ between $B \approx 3.8$ tesla to 7.3 tesla, and the transition from $N = 4$ to $N = 5$ between $B \approx 7.3$ tesla to 9 tesla are geometrically blockaded.

3 Results and Discussion

3.1 Ring-shaped QD

The exact diagonalization of the ring-shaped QD produces the many-body ground state configurations schematically shown in Fig. 1, as a function of magnetic field B. In order to make the interpretation easier, only those states which have different spin and spatial configuration are shown. Configurations in Fig. 1 represent the most relevant Slater determinants which contribute to the ground state in the corresponding ranges of field. The QD is symbolized with two semi-circles, the inner circle represents the core region (central potential minimum), and the outer circle represents the peripheral region (outer potential minimum). The arrows indicate spin states of the electrons occupying the regions. The thick black lines represents forbidden transitions between a $(N-1)$-electron QD and a N-electron QD. For instance, for the 5-electron QD, in the region between $B = 0 - 2$ tesla, the spin blockade occurs, *i.e.* the ground state transition from the 4-electron QD to the 5-electron QD involves changing the total spin of the QD by more than $1/2$, which has zero probability.

Most interesting, however, is the finding that there is another forbidden transition going from the 3-electron QD to the 4-electron QD in the field range $B \approx 3.2 - 6.8$ tesla. This is *not* due to spin blockade because the total spin is changed by only $1/2$. Our investigation indicates that this a new blockade regime that is induced by the fact that electrons can be localized in the two potential minima. Therefore, to add one electron to the 3-electron QD, the $3 \rightarrow 4$ transition requires the addition of a new electron plus a redistribution of one core electron to the peripheral region. The transition probability of such a process is proportional to that given by the spectral function $\Delta(N) \sim \sum_i |\langle N|c_i^\dagger|N-1\rangle|^2$ which turns out to be practically zero. To understand why is this, we denote the 4-electron QD wave function as $|c,c,,p,p>$ indicating that there are two core electrons (c) and two peripheral electrons (p), and the 3-electron QD wave function after one more electron is added as $|c,c,c,X\rangle$, which indicates the three original core electrons and the newly added electron in region X where $X = c$ or $X = p$. Therefore the spectral function is $\Delta = \sum_i |\langle c,c,p,p|a_i^\dagger|c,c,c\rangle|^2 \sim |\langle c,c,p,p|c,c,c,X\rangle|^2$. This transition probability is extremely small because mixing between Slater states with different localization configuration is extremely small (smaller than 0.1%) due to the spatial separation of the single particle states that make up the many-body Slater determinants. Such a *geometry induced blockade* is near 100% complete: it would greatly reduce the tunneling current when it occurs.

Another interesting result is how the spatial separation of electrons correlate with the orbital and spin degrees of freedom. Returning to Fig. 1, for 2-electron wave functions, our calculations show that the only effect of potential distortion is to push the singlet-to-triplet transition to near 7 tesla from ~ 3 tesla when there is no distortion. A large field is needed for our distorted dot because of the larger energy gap between core states which makes the change of an electron from $m = 0$ to $m = 1$ more difficult. For three electrons the effect is more striking: the peripheral and core regions are in competition for the third electron. At low field, the third electron (keeping in mind that we are using single electron language in these discussions) has two possibilities: it may reside in the core region and occupy the next single particle state, or it may reside in the peripheral region. For our QD, it turns out that the ground state is for the third electron to reside in the peripheral region at low B, because of the large energy gap between the core states at low B so that the third electron rather enters the peripheral region even though that region is a higher potential minimum. Another reason is that a reduction of total Coulomb interaction occurs when the third electron goes into the outer region of the QD. As B increases, the energy gap between the core states decreases, and as a result, an abrupt *redistribution* of an electron into the core region occurs at $B \sim 3.8$ tesla. For the 4-electron QD at $B < 2$ tesla, there are two electrons in the core and two in the peripheral region with total spin minimized. At ~ 2 tesla, the outer electrons become spin polarized. Then, at ~ 7 tesla, a transition between the two local potential minima occurs by which an outer electron redistributes into the core region. For the 5-electron QD, the localization configuration does not change in the magnetic field range studied here, *e.g.* there are two electrons in the core and three in the peripheral regions all the way to $B = 9$ tesla.

In Fig. 2 we plot the addition spectra as function of B.

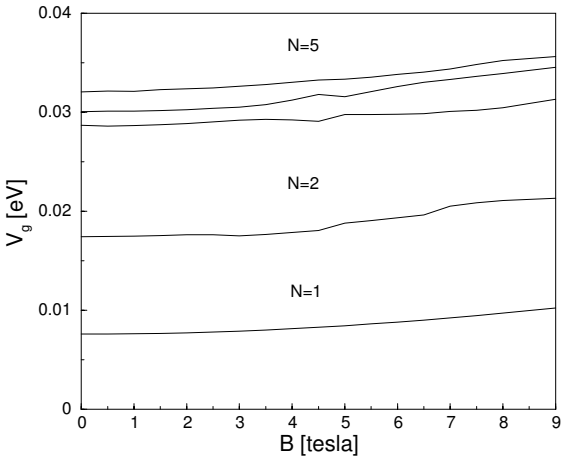

Figure 2. The addition spectra (chemical potential) of a strongly distorted QD as a function of B. The charging energy is substantially reduced after $N = 3$ due to spatial localization of electrons.

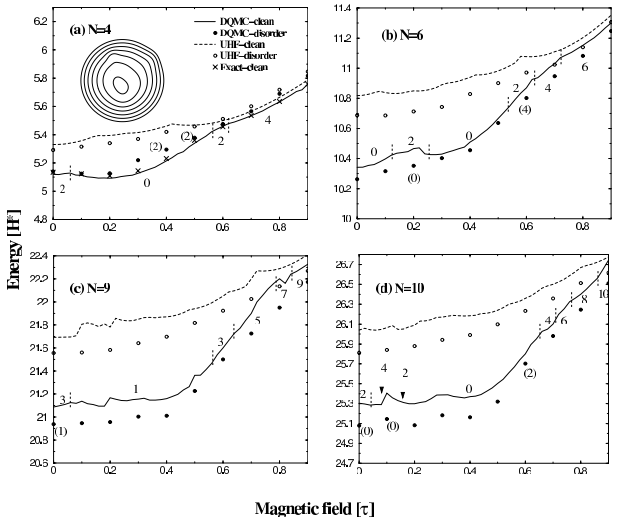

Figure 3. Many-body ground state energy as a function of magnetic field for (a) 4 electrons, (b) 6 electrons, (c) 9 electrons, and (d) 10 electrons. DQMC results are shown by solid lines (clean QD) and filled circles (disordered QD); UHF results are shown by dashed lines (clean QD) and open circles (disordered QD). For 4 electrons QD, exact results are also shown. The inset represents the confining potential of the first disordered QD (see Fig. 1) and walker positions for $B = 0.9\,\tau$ and $N = 4$.

The first 3 electrons enter the QD with an addition energy between $8 - 10$ meV. However, the next electrons have addition energies which are decreased considerably. There are several reasons for this behavior. First, interaction between electrons sitting in different potential minima is much weaker, only about 2 meV (with essentially no exchange energy due to weak wave function overlap). The direct Coulomb energy between peripheral states is low, ~ 3 meV, because they lie on large orbitals; whereas the attractive exchange energy between the nearest peripheral states can be as high as 1.5 meV due to their substantial overlap. In addition, as mentioned earlier, the energy difference between the lowest peripheral states are smaller than 0.1meV. As a result, the overall addition energy for 4 and 5 electrons is about $1 - 3$ meV.

3.2 Disordered QD

In Fig. 3 we present ground state energies obtained by UHF and DQMC for $N = 4, 6, 9,$ and 10 electrons for a given disorder configuration. In these calculations we use effective atomic units determined by taking into account the effective mass and dielectric constant of GaAs. This gives an effective Bohr radius $a_0^* = 9.793$ nm and an effective Hartree $\mathrm{H}^* = 11.86$ meV. For magnetic field, we use the unit defined by $\tau = (m^*/m_0\kappa)^2(\epsilon_0/2\mu_B)$ T which gives 6.862 T for the material parameters considered here. Here DQMC results are represented by solid lines for clean QD and filled circles for disordered QD; UHF results are represented by dashed lines for clean QD and open circles for disordered QD. For comparison, we also include results of exactly diagonalizing the many-body Hamiltonian H for $N = 4$ electrons in a disorder-free QD. The vertical dashed lines represent spin transitions as obtained by DQMC for clean QD, and total spin in the z-direction ($2 \times S_z$) are also indicated as integers in different magnetic field ranges separated by the vertical dashed lines. The numerical numbers in parenthesis are spins for states of disordered QD, and are indicated only if they differ from the clean QD results. The shaded area in the confining potential indicate the random walker positions in our DQMC simulation at $B = 0.9\,\tau$ and $N = 4$.

First, we consider results for clean-QD's. We have verified that results from exact diagonalization and DQMC agree very well, as shown in Fig. 3(a) for a clean QD with $N = 4$ electrons. The DQMC results are actually *lower* by $\sim 0.03\,\mathrm{H}^*$ in the low-field region, indicating a slightly better convergence of the DQMC results. The exact diagonalization produced a slightly higher energy in the range of B-field presumably due to the limited number of Landau levels used in our analysis[55], but the agreement between DQMC and exact diagonalization is very satisfactory. In the maximum density droplet[57,44] (MDD) region, *i.e.* $B > 0.6\,\tau$, results from DQMC and exact diagonalization become indistinguishable[56]. The essentially perfect agreement in the MDD region is not surprising since the MDD state has a very small correlation energy and is well approximated by a single Slater determinant. This is also the reason that UHF results are rather close to the DQMC/exact results in the MDD state, see Fig. 3(a). However, for lower magnetic fields it is well known that the HF method does not give accurate energies and correct spin states[10], as clearly seen in Fig. 3 for up to ten electrons. Our DQMC results for 6 electrons in a clean QD (solid line of Fig. 3(b)) agree well with a previous variational QMC calculations[32]: our re-

sults give the same spin transition sequences of $0 \rightarrow 2 \rightarrow 0 \rightarrow 2 \rightarrow 4 \rightarrow 6$ with an increasing magnetic field. For $N = 9$ and $N = 10$ clean-QD's, spin transition sequences are found to be $3 \rightarrow 1 \rightarrow 3 \rightarrow 5 \rightarrow 7 \rightarrow 9$ and $0 \rightarrow 2 \rightarrow 0 \rightarrow 4 \rightarrow 0 \rightarrow 2 \rightarrow 0 \rightarrow 4 \rightarrow 6 \rightarrow 8 \rightarrow 10$ as seen in the Fig. 3(c) and (d), respectively. The spin states which appear for very small magnetic field windows are shown by arrows in Fig. 3(d).

Next, we discuss the disorder effects shown in Fig. 3. The most striking result is the deformation caused by disorder in energy as a function of magnetic field. For instance, the energy difference between clean QD and disordered QD for $N = 6$ is about 0.1 H* at $B = 0.2\,\tau$, while it is about 0.02 H* at $B = 0.3\,\tau$, as shown in Fig. 3(b). Due to these differences, the structures in the $E = E(B)$ curve, which are caused by different spin or momentum transitions, are drastically reduced for disordered QD. Such an effect is also observed for other electron numbers, and can make experimental observation of many-body transitions difficult. Analyzing the spin transitions, we find that disorder can strongly affect the total spin. For instance, in a 4-electron QD, $0 \rightarrow 2$ transition occurs at much smaller B (see Fig. 3(a)), and in the 10-electron QD, $S_z = 2$ state appears at $B = 0.6\,\tau$, while no such a state exists in the corresponding clean QD.

In atomic physics, Hund's rule determines whether a spin-down or a spin-up electron is added in order to fill the shells sequentially. For closed shells, *i.e.* at atomic numbers (magic numbers) 2, 10, 18,..., total spin must be zero. For any other atomic numbers, total spin in the open shell must be maximized. Due to the cylindrical symmetry, the magic numbers for the QD system we are studying are 2, 6, 12,... Experimentally, magic numbers as well as the half-shell electron numbers (4, 9,...) can be observed since they are responsible for maxima in addition energies in QD's[53,54]. The stability of Hund's rule against elliptical deformation[28], random disorder[31] and non-parabolicity of the confinement potential[54] were tested by density functional theories[28,31,54].

In Fig. 3, we show addition energy up to 13 electrons at zero magnetic field, calculated for a clean QD (the lowest line) and 8 different disorder configurations following the order presented in Fig. 1 (2nd line and up). It is clear that closed shell structures are not affected by disorder at least for the disorder strengths we have used, giving a higher peak at magic numbers $N = 2, 6$ and 12 corresponding to closed shells. On the other hand, although the half-shell peak at $N = 4$ is not affected by disorder, the half-shell peak at $N = 9$ is found to be less robust against disorder. Our calculations show that for the eight disordered QD's we investigated, the $9-$th peak is an energy minimum in four of them; in addition, statistical noise in the DQMC calculation prevented us from reaching conclusive results for another three QD's. Finally, we note that a very clear dip at $N = 11$ is observed in all our results.

In Fig. 4, the numbers on the lowest spectrum represents $2 \times S_z$ for different N. For disordered QD's, S_z is plotted only if it differs from the clean QD case. According to Hund's rule, the total spin must be maximized in the outer shell. Moreover, it is believed that, in disordered QD's, high-spin states are suppressed due to a lifting of degeneracy [31]. We note that since we are using single Slater determinants, only z component of the total spin can be resolved, and so in the following, we limit our discussions to S_z. Without disorder, our DQMC results are in perfect agreement with Hund's rule. When disorder is added, we found that Hund's rule is especially stable for closed shells as well as for the second open shell ($N = 3, 4, 5$). For the third open shell ($N = 7 - 11$), Fig. 4 shows that there are some deviations in S_z from that of the clean QD, especially for $N = 10$ where $S_z = 0$ was found in five out of the eight disordered QD's, different from the $S_z = 2$ for the clean QD. A higher probability of $S = 0$ state for $N = 10$ was also found in density functional calculations[31]. These results also show that maximal spin alignment does not guarantee a peak at half-shell filling in agreement with density functional calculations[54] as seen, for instance, in the disorder configuration number two. Other deviations from the clean QD case are observed for the third shell of disordered QD number one; spin is minimized for $N = 7$, 8, and 9 QD's.

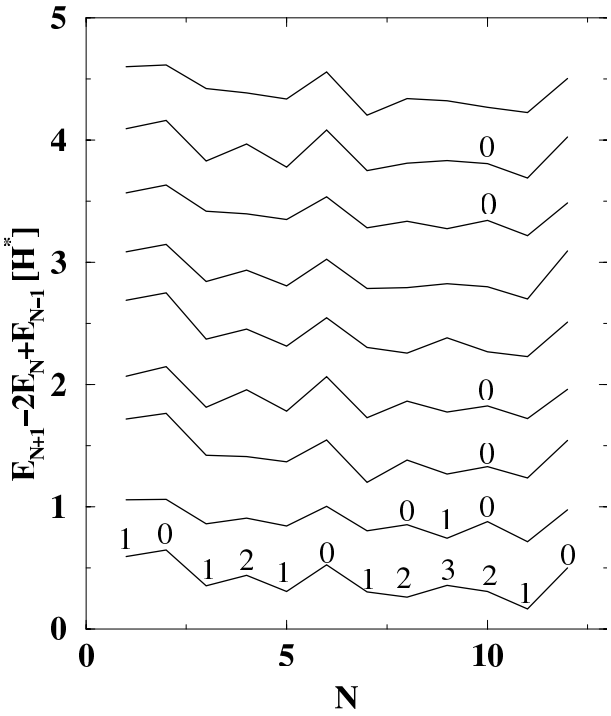

Figure 4. Addition energy at $B = 0$ up to 13 electrons for clean QD (the lowest line) and 8 different disorder configuration following the order represented in Fig. 1 (2nd line and up). The numbers represent $2 \times S_z$, and they are shown for disordered QD's only if they differ from the clean QD results.

4 Conclusion

To summarize, We have investigated the competing energetics of electron-electron interaction, magnetic field, and geometrical factors, in quantum dots with up to thirteen electrons, using exact numerical techniques such as exact diagonalization and DQMC. The ring-shaped potential landscape provides a competition of various contributions to the total energy by spatially separating electrons. Such effects have interesting implications for tunneling current in the Coulomb blockade regime, at least for cases involving a small number of strongly interacting electrons as we have studied. By localizing in different potential minima, the total ground state energy is minimized. However, due to the energetics competition, adding an electron to the QD may involve a charge redistribution between the two potential minima. We found that this redistribution occurs abruptly as the magnetic field is increased. A most interesting outcome of the redistribution is a new blockade phenomenon which is caused by a drastic reduction of the spectral weight for the transition from a $(N-1)$-electron QD to a N-electron QD due to the spatial localization of the electrons. The geometric blockade leads to a drastic reduction of the tunneling current which should be measurable experimentally.

DQMC is shown to give excellent total energy and spin configuration for clean-QD's as compared with exact diagonalization, and is very powerful for investigating disordered QD's which do not possess any spatial symmetry. The lack of spatial symmetry makes an exact calculation very difficult if not impossible for $N > 7$, even for modern computers. Compared with the UHF technique, DQMC gives superior advantages in total energy accuracy, especially for low magnetic field before the transition to maximum density droplet states. Disorder is found to have very significant effects to the total energy of QD. In particular, the energetic transition (the kinks in energy) between many-body states is made much less clear due to disorder, and the required magnetic field to induce such transitions may be rather different than that of clean-QD, this may have important implications to interpreting tunneling spectroscopy data. We found that Hund's rule for closed shell is robust against even strong disorder, but less so for open shells. For the lower shells, the spin states are largely unaffected by disorder, but for higher shells (larger number of electrons N) this may change due to disorder.

Acknowledgments

We gratefully acknowledge financial support from Natural Science and Engineering Research Council of Canada, le Fonds pour la Formation de Chercheurs et l'Aide à la Recherche de la Province de Québec, and NanoQuebec. We gratefully acknowledge Prof. J.S. Wang for helping us in developing the DQMC code, and we thank Dr. Pawel Hawrylak for several useful discussions on spin configurations and Hund's rule of quantum dots.

References

1. See, for example, articles in *Mesoscopic Electron Transport*, edited by L.L. Sohn, L.P. Kouwenhoven and G. Schön, (Kluwer, Series E 345, 1997).
2. R.C. Ashoori, Nature (London) **379**, 413 (1996).
3. R.C. Ashoori, H.L. Stormer, J.S. Weiner, L.N. Pfeiffer, S. J. Pearton, K.W. Baldwin, and K.W. West, Phys. Rev. Lett. **68**, 3088 (1992).
4. R.C. Ashoori, H.L. Stormer, J.S. Weiner, L.N. Pfeiffer, K.W. Baldwin, and K.W. West, Phys. Rev. Lett. **71**, 613 (1993).
5. L. P. Kouwenhoven, T. H. Oosterkamp, M. W. S. Danoesastro, M. Eto, D. G. Austing, T. Honda, and S. Tarucha, Science **278**, 1788 (1997).
6. P.A. Maksym, and T. Chakraborty, Phys. Rev. Lett. **65**, 108 (1990).
7. U. Merkt, J. Huser, and M. Wagner, Phys. Rev. B **43**, 7320 (1991).
8. N.F. Johnson, and M.C. Payne, Phys. Rev. B **45**, 3819 (1992).
9. S.R.Eric Yang, A.H. MacDonald, and M.D. Johnson, Phys. Rev. Lett. **71**, 3194 (1993).
10. J.J. Palacios, L. Martin-Moreno, G. Chiappe, E. Louis, C. Tejedor, Phys. Rev. B **50**, 5760 (1994);
11. A. Wojs, and P. Hawrylak, Phys. Rev. B **56**, 13227 (1997).
12. J.J. Palacios, P. Hawrylak, Physical Rev. B **51**, 1769 (1995).
13. R. Berkovits, Phys. Rev. Lett. **81**, 2128 (1998).
14. C.M. Canali, Phys. Rev. Lett. **84**, 3934 (2000).
15. M. Fujito, A. Natori, and H. Yasunaga, Phys. Rev. B **53**, 9952 (1996).
16. H.-M. Muller, and S.E. Koonin, Phys. Rev. B **54**, 14532 (1996).
17. H. Tamura, and M. Ueda, Phys. Rev. Lett. **79**, 1345 (1997).
18. K.-H. Ahn, K. Richter, and In-Ho Lee, Phys. Rev. Lett. **83**, 4144 (1999).
19. C. Yannouleas, and U. Landman, Phys. Rev. Lett. **82**, 5325 (1999).
20. A. Cohen, K. Richter, and R. Berkovits, Phys. Rev. B **60**, 2536 (1999).
21. S. Levit, and D. Orgad. Phys. Rev. B **60**, 5549 (1999).
22. M.-C. Cha, and S.-R. Eric Yang, Phys. Rev. B **61**, 1720 (2000).
23. D. Ullmo, and H.U. Baranger, Phys. Rev. B **64**, 245324 (2001).
24. B. Reusch, W. Hausler, and H. Grabert **63**, 113313 (2001).
25. M. Koskinen, and M. Manninen, and S. M. Reimann, Phys. Rev. Lett. **79**, 1389 (1997).
26. S. M. Reimann, M. Koskinen, J. Helgesson, P.E. Lindelof, and M. Manninen, Phys. Rev. B **58**, 8111 (1998).
27. O. Steffens, U. Rossler, and M. Suhrke, Europhys. Lett. **42**, 529 (1998).
28. K. Hirose, and N. S. Wingreen, Phys. Rev. B **59**, 4604 (1999).
29. C. A. Ullrich, and G. Vignale, Phys. Rev. B **61**, 2729 (2000).
30. K. Hirose, F. Zhou, and N. S. Wingreen, Phys. Rev. B **63**, 075301 (2001).
31. K. Hirose, and N. S. Wingreen, Phys. Rev. B **65**, 193305 (2002).
32. H. Saarikoski, E. Rasanen, S. Siljamake, A. Harju, M. J. Puska, and R. M. Nieminen, Eur. Phys. J. B **26**, 241 (2002).
33. F. Bolton, Phys. Rev. B **54**, 4780 (1996).
34. Y. Wan, G. Ortiz, and P. Phillips, Phys. Rev. B **55**, 5313 (1997).
35. E. Lee, A. Puzder, M. Y. Chou, T. Uzer, and D. Farrelly, Phys.

Rev. B **57**, 12281 (1998).
36. A. Harju, V. A. Sverdlov, and R. M. Nieminen, Europhys. Lett. **41**, 407 (1998).
37. A. Harju, V. A. Sverdlov, R. M. Nieminen, and V. Halonen, Phys. Rev. B **59**, 5622 (1999).
38. A. Harju, S. Siljamaki, and R. M. Nieminen, Phys. Rev. B **60**, 1807 (1999).
39. R. Egger, W. Hausler, C. H. Mak, and H. Grabert, Phys. Rev. Lett. **82**, 3320 (1999).
40. F. Pederiva, C. J. Umrigar, and E. Lipparini, Phys. Rev. B **62**, 8120 (2000).
41. S.-R. Eric Yang, M.-C. Cha, and J. H. Han, Phys. Rev. B **62**, 8171 (2000).
42. J. Harting, O. Mulken, and P. Borrmann, Phys. Rev. B **62**, 10207 (2000).
43. L. Coletti, F. Pederiva, E. Lipparini, and C. J. Umrigar. Eur. Phys. J. B **27**, 385 (2002).
44. S. Siljamaki, A. Harju, R. M. Nieminen, V. A. Sverdlov, and P. Hyvonen, Phys. Rev. B **65**, 121306 (2002).
45. K. S. Liu, M. H. Kalos, and G. V. Chester, Phys. Rev. A **10**, 303 (1974).
46. G. Ortiz, D. M. Ceperley, and R. M. Martin, Phys. Rev. Lett. **71**, 2777 (1993).
47. C. J. Umrigar, M. P. Nightingale, and K. J. Runge, J. Chem. Phys. **99**, 2865 (1993).
48. W. M. C. Foulkes, L. Mitas, R. J. Needs, and G. Rajagopal, Rev. Mod. Phys. **73**, 33 (2001).
49. N.B.Zhitenev, R.C. Ashoori, L.N. Pfeiffer, and K.W. West, Phys. Rev. Lett. **79**, 2308 (1997).
50. M. Brodsky, N.B. Zhitenev, R.C. Ashoori, L.N. Pfeiffer, and K.W. West, Phys. Rev. Lett. **85**, 2356 (2000).
51. L.P. Rokhinson, L.J. Guo, S.Y. Chou, and D.C. Tsui , Phys. Rev. B **63**, 035321 (2001).
52. S. Luscher, T. Heinzel, K. Ensslin, W. Wegscheider, and M. Bichler, Phys. Rev. Lett. **86**, 2118 (2001).
53. S. Tarucha, D. G. Austing, and T. Honda, R. J. van der Hage, and L. P. Kouwenhoven, Phys. Rev. Lett. **77**, 3613 (1996).
54. P. Matagne, J. P. Leburton, D. G. Austing, and S. Tarucha, Phys. Rev. B **65**, 85325 (2002).
55. In our exact diagonalization calculation, we have used three Landau levels for $B < 5\ \tau$, and two Landau levels for $B > 5\ \tau$, to obtain numerical convergence of the results.
56. The statistical noise of our DQMC results vary between 0.003 and 0.01 H^*, depending on values of electron number N, the magnetic field B, and the total spin S_z. The statistical noise at the MDD region is about 0.003 H^*.
57. T.H. Oosterkamp, J.W. Janssen, L.P. Kouwenhoven, D.G. Austing, T. Honda, and S. Tarucha, Phys. Rev. Lett. **82**, 2931 (1999).
58. T. Chakraborty, and P. Pietilainen, Phys. Rev. B **50**, 8460 (1994).
59. K. Varga, P. Navratil, J. Usukura, and Y. Suzuki, Phys. Rev. B **63**, 205308 (2001).
60. A. Emperador, M. Barranco, E. Lipparini, M. Pi, and L. Serra, Phys. Rev. B **59** 15301 (1999).
61. A. D. Guclu, Q. F. Sun, H. Guo, and R. Harris, Phys. Rev. B. **66**, 195327 (2002).
62. V. Fock, Z. Phys. **47**, 446 (1928); C.G. Darwin, Proc. Cambridge Philos. Soc. **27**, 86 (1930).